

# Experimental and Modeling Studies of the Degradation of Estrogen Hormones in Aqueous TiO<sub>2</sub> Suspensions under Simulated Solar Radiation

Zacharias Frontistis,<sup>†</sup> Catherine Drosou,<sup>†</sup> Konstantina Tyrovola,<sup>†</sup> Dionissios Mantzavinos,<sup>†,§</sup> Despo Fatta-Kassinos,<sup>‡,§</sup> Danae Venieri,<sup>†</sup> and Nikolaos P. Xekoukoulotakis<sup>†,\*</sup>

<sup>†</sup>Department of Environmental Engineering, Technical University of Crete, Polytechniopolis, GR-73100 Chania, Greece

<sup>‡</sup>Department of Civil and Environmental Engineering, University of Cyprus, P.O. Box 20537, 1678 Nicosia, Cyprus

<sup>§</sup>NIREAS—International Water Research Center, P.O. Box 20537, 1678 Nicosia, Cyprus

**ABSTRACT:** The efficiency of TiO<sub>2</sub> photocatalysis to degrade three estrogen hormones, that is, 17 $\alpha$ -ethynylestradiol (EE2), estrone (E1), and 17 $\beta$ -estradiol (E2), in environmentally relevant samples was investigated. Radiation at a photon flux of  $1.7 \times 10^{-7}$  einstein/s was provided by a solar simulator and experiments were conducted at various TiO<sub>2</sub> loadings (25–1500 mg/L), estrogen concentrations (85–300  $\mu$ g/L in individual solutions and 400  $\mu$ g/L in mixture), and water matrices (ultrapure water, drinking water, and secondary treated wastewater). Changes in estrogen concentration were followed by high performance liquid chromatography and estrogenicity by the yeast estrogen screening assay. Aeroxide P25, a commercially available mixture of 75:25 anatase/rutile, was considerably more active than carbon-doped and undoped anatase titania, with degradation increasing with increasing catalyst loading and treatment time. The organic and inorganic constituents typically found in wastewater and drinking water impeded degradation presumably due to the scavenging of oxidizing species. For example, the time needed for complete 100  $\mu$ g/L EE2 degradation in pure water was an order of magnitude lower than that in wastewater. The three estrogens exhibited comparable reactivity, with E1 being slightly more reactive than the rest. Degradation in multicomponent mixtures was slower than in individual solutions, thus implying estrogen competition for oxidizing species. Although the mixture of three in wastewater could be degraded fully after 120 min, overall estrogenicity was reduced by just about 30%, highlighting the role of the complex water matrix. Several oxidation products of EE2 were identified by means of LC–MS/MS and a reaction network for the photocatalytic degradation of EE2 is suggested. An artificial neural network comprising five input variables (reaction time, TiO<sub>2</sub> and EE2 concentration, organic content, and conductivity of the water matrix), eight neurons and an output variable (conversion) was optimized, tested, and validated for EE2 degradation. The network, based on tangent sigmoid and linear transfer functions for the hidden and input/output layers, respectively, and the Levenberg–Marquardt back-propagation training algorithm, can successfully predict EE2 degradation.

## 1. INTRODUCTION

**1.1. The Specific Problem.** Endocrine disrupting compounds (EDCs) constitute a family of emerging microcontaminants that have the ability to interact with the endocrine system of the organisms, thus causing various developmental and reproductive disorders, including feminizing effects. EDCs include estrogen hormones (man-made and naturally occurring), phyto-estrogens and industrial chemicals, with the former being far more estrogenically potent than the other.<sup>1</sup> EDCs, as well as other microcontaminants, are only partially removed in conventional wastewater treatment plants (WWTP) and the discharged residuals may re-enter the water cycle.<sup>2</sup> Several monitoring campaigns<sup>3–5</sup> have reported the presence of naturally occurring estrone (E1) and 17 $\beta$ -estradiol (E2), as well as synthetic 17 $\alpha$ -ethynylestradiol (EE2) in WWTP influents and discharges at the ng/L level. The main physical, biological, and advanced oxidation processes for the removal of estrogenic steroid hormones from water have been recently reviewed.<sup>6</sup>

**1.2. Research Context.** Semiconductor photocatalysis has been extensively and successfully employed for the degradation of a wide range of microcontaminants in waters and

wastewaters. TiO<sub>2</sub> is the most promising photocatalyst due to its high photocatalytic efficiency; in addition, it is relatively cheap, commercially available in various crystalline forms and particle characteristics, nontoxic, and photochemically stable.

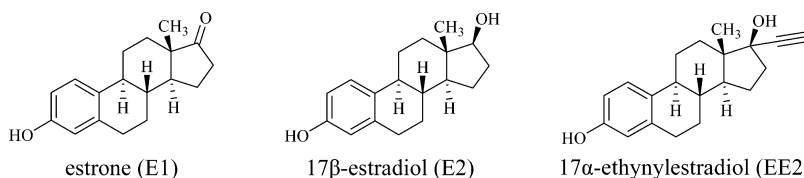
TiO<sub>2</sub> photocatalysis has been employed to degrade a mixture of E1 and E2 in model aqueous solutions concerning the effect of operating conditions (*i.e.*, radiation wavelength, pH, catalyst, and H<sub>2</sub>O<sub>2</sub> concentration) on kinetics.<sup>7</sup> In other studies,<sup>8</sup> a synthetic solution of E1, E2, EE2, and estriol was subject to TiO<sub>2</sub> photocatalysis under UV-C or UV-A radiation in an annular photoreactor to model the radiation field and, subsequently, develop kinetic expressions independent of the reactor geometry and field. EE2 in pure water or in a water/methanol mixture was photocatalytically oxidized to identify its major transformation intermediates and suggest possible degradation pathways.<sup>9</sup> The effect of adding ethanol and/or urea in aqueous solutions of E2 and EE2 on the extent of

**Received:** March 1, 2012

**Revised:** November 6, 2012

**Accepted:** December 4, 2012

**Published:** December 4, 2012

Scheme 1. Chemical Structures of Estrone (E1), 17 $\beta$ -Estradiol (E2) and 17 $\alpha$ -Ethinylestradiol (EE2)

estrogen adsorption onto titania particles and subsequent photodegradation was evaluated in other studies.<sup>10</sup>

In addition, Ray and co-workers studied the photodegradation of E1 in aqueous solutions under simulated solar radiation and they determined the effects of several parameters such as E1 initial concentration, irradiation intensity, solution pH, effect of humic substances, and dissolved oxygen.<sup>11</sup> They found that E1 was degraded rapidly, with a half-life ranging from 48 to 123 min, depending on irradiation intensity and initial E1 concentration, while the maximum E1 degradation occurred for a humic acid content of 8 mg/L and at neutral solution pH. Moreover, they also studied the photodegradation of E2 in aqueous solutions under simulated solar radiation in the presence of various natural water constituents, such as  $\text{NO}_3^-$ ,  $\text{Fe}^{3+}$ ,  $\text{HCO}_3^-$ , humic acid, and turbidity.<sup>12</sup> They found that the photodegradation rate increased significantly in the presence of  $\text{NO}_3^-$ ,  $\text{Fe}^{3+}$ , and humic acid, which was attributed to the photochemical formation of hydroxyl radicals, as well as other reactive oxygen species. On the other hand, the reaction rate decreased markedly in the presence of  $\text{HCO}_3^-$ , which was attributed to the fact that bicarbonate acts as a hydroxyl radical scavenger.

**1.3. Aims and Novelty.** Although the aforementioned studies<sup>7–12</sup> are important describing mostly experimental work in the area, they have not addressed two serious points, namely: (i) the use of renewable energy to induce photochemical reactions in a sustainable way, since radiation was mostly provided by artificial UV lamps; (ii) the role of environmentally relevant, complex matrices since they have exclusively been carried out in model aqueous solutions and/or at conditions that are far from those typically met in environmental samples (e.g., presence of organic solvents, estrogen concentrations at the mg/L level, highly acidic or alkaline conditions, etc). In this context, the aim of our work was to study the  $\text{TiO}_2$  photocatalytic degradation of three estrogens (E1, E2, and EE2) under simulated solar radiation in model solutions, as well as in environmentally relevant samples with emphasis on the effect of the water matrix, catalyst type and concentration, estrogen concentration on degradation kinetics, and estrogenicity. An attempt was also made to elucidate reaction pathways and mechanisms of the photocatalytic degradation of EE2 through the identification of oxidation byproducts.

In addition to experimental work, artificial neural networks (ANN) were employed to simulate EE2 degradation and assess the importance of various operating variables. ANN are mathematical models and algorithms that have been designed to mimic the information processing and knowledge acquisition methods of the human brain. In recent years, ANN have been employed to model water/wastewater treatment processes although they are less popular than other modeling approaches; therefore, it is not surprising that ANN modeling of heterogeneous photocatalytic treatments has merely been reported in the literature.<sup>13</sup> Moreover, only a handful of studies have dealt with ANN models for solar-driven  $\text{TiO}_2$  processes

for the degradation of pharmaceuticals,<sup>14</sup> reactive dyes,<sup>15</sup> and effluents from a thermoelectric power station.<sup>16</sup>

## 2. EXPERIMENTAL SECTION

**2.1. Materials.** Estrone (E1:  $\text{C}_{18}\text{H}_{22}\text{O}_2$ ), 17 $\beta$ -estradiol (E2:  $\text{C}_{18}\text{H}_{24}\text{O}_2$ ) and 17 $\alpha$ -ethinylestradiol (EE2:  $\text{C}_{20}\text{H}_{24}\text{O}_2$ ), whose chemical structures are shown in Scheme 1, were purchased from Sigma-Aldrich and used as received. Humic acid,  $\text{NaHCO}_3$ ,  $\text{NaCl}$ ,  $\text{Na}_2\text{SO}_4$ ,  $\text{NaNO}_3$ ,  $\text{NaNO}_2$ , and  $\text{NaH}_2\text{PO}_4 \cdot \text{H}_2\text{O}$  were also purchased from Sigma-Aldrich and used as received. Aqueous solutions of the estrogens were prepared in four matrices, namely, (i) ultrapure water (UPW: pH = 6.1, 5.5  $\mu\text{S}/\text{cm}$  conductivity) taken from a water purification system (EASYPureRF-Barnstead/Thermolyne, USA); (ii) drinking water (DW: pH = 7.9, 308  $\mu\text{S}/\text{cm}$  conductivity, 152 mg/L bicarbonates) taken from the local water supply network; (iii) secondary treated wastewater (WW) collected after chlorination from the municipal WWTP of Chania, W. Crete, Greece. The effluent was characterized by standard methods<sup>17</sup> as follows: the chemical oxygen demand and dissolved organic carbon (DOC) was 24 and 8.4 mg/L, respectively, while its pH was 8 and the conductivity 810  $\mu\text{S}/\text{cm}$ . Moreover, it contained 172 mg/L chlorides, 194 mg/L bicarbonates, 54 mg/L sulfates, 37 mg/L nitrates, and 37 mg/L nitrites; (iv) WW diluted with an equal volume of UPW.

Stock solutions of the estrogenic compounds were prepared dissolving approximately 5 mg of the estrogen in 5 L of the water matrix by prolonged stirring (i.e., 1 to 3 days) at ambient conditions and in the dark as the compounds in question were not easily dissolved in water. The exact concentration of the resulting aqueous stock solutions was measured by HPLC (*vide infra*). The stock solutions were then diluted adding the corresponding water matrix to obtain the desired estrogen concentration which, in most cases, was in the range 85–300  $\mu\text{g}/\text{L}$ . These concentrations, although greater than those typically found in environmental samples, were chosen to allow (i) the assessment of process efficiency within a measurable time scale, and (ii) the accurate determination of residual estrogens concentration with the analytical techniques employed in this work (*vide infra*).

All chemicals needed for the YES bioassay were research-grade, suitable for cell culture, and they were purchased from Sigma-Aldrich.

Six commercially available  $\text{TiO}_2$  samples, with various crystal forms and particle characteristics, were employed for slurry photocatalytic experiments. Their main properties, according to the corresponding manufacturers, are summarized in Table 1. Diffuse reflectance spectra (DRS) of the catalysts were recorded in the range of 200–800 nm at room temperature using a UV–vis spectrophotometer (Varian Cary 3) equipped with an integration sphere.

**2.2. Photocatalytic Experiments.** Photocatalytic experiments were performed using a solar radiation simulator (Newport, model 96000) equipped with a 150 W xenon

**Table 1.** TiO<sub>2</sub> Catalysts Used in the Present Study: A, Anatase; R, Rutile

catalyst	doping	crystal form	specific surface area, m <sup>2</sup> /g	average primary particle size, nm	supplier
Aeroxide P25	none	A:R 75:25	50 ± 15	21	Evonik Industries
Hombikat UV 100	none	A	348	16	Sachtleben Chemie
Kronos vlp 7000	carbon	A	>225	15	Kronos Worldwide
Kronos vlp 7001	carbon	A	>225	15	Kronos Worldwide
Kronos vlp 7100	carbon	A	>80	15	Kronos Worldwide
Kronos vlp 7101	carbon	A	>125	15	Kronos Worldwide

ozone-free lamp and an Air Mass 1.5 Global Filter (Newport, model 81094), thus simulating solar radiation reaching the surface of the earth at a zenith angle of 48.2°. The diameter of the solar beam was 2.2 cm. According to the spectral irradiance data given by the manufacturer (Newport), simulated solar radiation contains about 5% UV-A radiation, and 0.1% UV-B irradiation, while the filter cuts radiations with wavelengths lower than 280 nm. The incident photon flux on the photochemical reactor in the UV region of the electromagnetic spectrum was measured actinometrically using 2-nitrobenzaldehyde (purchased from Sigma-Aldrich) as the chemical actinometer<sup>18,19</sup> and it was found to be  $1.7 \times 10^{-7}$  einstein/s.

Reactions took place in an open, double-walled, cylindrical glass vessel. The inner diameter of the reaction vessel was 7.8 cm. In a typical photocatalytic run, 300 mL of the aqueous solution containing the desired concentration of estrogens were loaded in the reaction vessel. The depth of the solution inside the reactor was 6.2 cm. The solution was slurried with the appropriate amount of catalyst and magnetically stirred in the dark to ensure complete equilibration of adsorption/desorption of estrogens onto the TiO<sub>2</sub> surface, which was complete after 30 min. After that period, the solar simulator was turned on and the reaction mixture was exposed to simulated solar radiation under continuous stirring. During photocatalytic experiments, temperature was maintained constant at  $25 \pm 1$  °C with a temperature control unit. Unless otherwise stated, the reaction mixture was exposed to ambient air and no further aeration took place. All the experiments were performed at inherent solution pH, which was left uncontrolled during the reaction. Runs were performed in duplicate and mean values are quoted as results (relative standard deviation was typically less than 5%). Conversion and reaction rates were computed relative to the measured estrogen concentration after the 30-min dark adsorption period rather than its initial value prior to equilibration.

**2.3. Analytical Techniques.** Samples periodically taken from the reaction vessel were centrifuged at 13200 rpm to remove catalyst particles and then analyzed for residual estrogens concentration. The latter was followed by high performance liquid chromatography (Waters Alliance 2690 HPLC system) employing a Luna C18(2) column (5 µm, 4.6 mm × 250 mm) and a security guard column (4 mm × 3 mm) both purchased from Phenomenex, and two detectors connected in series, namely a diode array detector (Waters 2996 PDA detector) and a fluorescence detector (Waters 474 Scanning Fluorescence detector). The mobile phase was a

mixture of ultrapure water and acetonitrile in 35:65 volumetric ratio eluted isocratically at a flow rate of 1 mL/min. The injection volume was 100 µL and the column was thermostatted at 30 °C. E2 and EE2 were detected by the fluorescence detector, in which the excitation wavelength was 280 nm and the emission wavelength was 305 nm, while E1 was detected by the diode array detector set at 220 nm. Under these conditions, the retention time was 5.7, 4.6, and 5.1 min for E1, E2, and EE2, respectively. Calibration curves were constructed preparing standard solutions of the estrogen compounds. The limit of detection was 2.95, 0.59, and 0.63 µg/L for E1, E2, and EE2, respectively, while the limit of quantitation was 9.83, 1.95, and 2.11 µg/L for E1, E2, and EE2, respectively.

EE2 photocatalytic degradation products were separated and identified by liquid chromatography tandem mass spectrometry (LC-MS/MS). LC was performed with a Waters Alliance 2695 HPLC system employing the above-mentioned Luna C18(2) column. The mobile phase was a mixture of ultrapure water acidified with 0.1% acetic acid and acetonitrile using a gradient program. The gradient started with 20% acetonitrile and proceeded to 80% acetonitrile over 15 min, conditions hold for 2 min, returned back to the starting conditions over 2 min, followed by equilibration for 15 min. The flow rate was 1 mL/min, however the flow was split and reduced to 0.4 mL/min before entering the mass spectrometer. The injection volume was 100 µL. Tandem mass spectrometry was performed on a benchtop triple quadrupole Quattro micro MS from Waters-Micromass (Manchester, UK) equipped with an electrospray probe and a Z-spray interface. MS measurements were performed in positive ionization mode and in the multiple reaction monitoring (MRM) mode. High purity nitrogen was used for desolvation and nebulization. The MS parameters were optimized by directly infusing a solution of EE2 dissolved in ultrapure water acidified with 0.1% acetic acid and acetonitrile 50/50 v/v, into the electrospray probe with a syringe pump at an infusion rate of 20 µL/min. Desolvation was carried out at 450 °C with a desolvation gas flow of 300 L/h. The source temperature was set to 120 °C and the cone gas flow was 50 L/h. Other parameters optimized for the MS measurements were as follows: capillary voltage 3.80 kV in the positive mode, cone voltage 20 V, extractor voltage 2 V, multiplier voltage 650 V. Instrument control, data acquisition and evaluation was performed with MassLynx software (Waters).

DOC was measured on a Shimadzu S000A TOC analyzer whose operation is based on nondispersive infrared gas analysis.

**2.4. Yeast Estrogen Screening (YES).** The YES bioassay was employed to assess the effect of photocatalytic treatment on estrogenicity. The assay was carried out according to the procedures described in detail elsewhere<sup>20</sup> with some modifications. In brief, standard solutions and sample extracts were produced in ethanol and 10 µL of dilution series were dispensed into triplicate wells of 96-well microtiter plates. After evaporation to dryness at room temperature, 0.2 mL of growth medium containing chlorophenol red-b-D-galactopyranoside and the yeast cells were added, followed by incubation at 32 °C for 72 h. Each plate contained at least one row of blanks and a standard curve for E2, ranging from 3 µg/L to 1.5 ng/L. During the incubation period, the microtiter plates were shaken at 80 rpm for 2 min to mix and disperse the growing cells. The absorbance of the medium was measured using a microplate reader (LT-4000MS Microplate Reader, Labtech) and Manta PC analysis software. The absorbance at 540 nm was regarded as estrogenic activity after subtraction of absorbance at 640 nm



to correct for yeast growth. Positive wells are indicated by a deep red color and by turbid yeast growth.

**2.5. Artificial Neural Network (ANN).** A computational neural network consists of numerous individual processing units called neurons, which are grouped into layers and put in relation to each other by parallel connections. The strength of these interconnections is determined by the weight associated with the neurons.<sup>13</sup> In this work, a three-layered back-propagation ANN was chosen comprising an input layer (independent variables), an output layer (dependent variable), and a hidden layer. A tangent sigmoid (tansig) transfer function was employed to activate the hidden layer, while a linear (purelin) function for the input/output layers. The Levenberg–Marquardt back-propagation algorithm was chosen for training purposes; more details regarding transfer functions and the training algorithm can be found elsewhere.<sup>13</sup>

The input layer includes five variables which are shown in Table 2 alongside the respective range of values, while EE2

**Table 2. Range and Relative Significance of the ANN Input Variables Used in This Work**

input variable	range	significance, %
reaction time	0–120 min	45.3
Aeroxide P25 loading	15–1500 mg/L	17.5
EE2 concentration	85–300 µg/L	10.5
water matrix DOC	0–8.4 mg/L	10.5
water matrix conductivity	5.5–810 µS/cm	16.2
total		100

conversion is the dependent variable of the output layer. A set of 169 experimental data were divided into training (70%, 119 data), validation (15%, 25 data), and test (15%, 25 data) subsets. The Neural Network Toolbox of Matlab R2011 mathematical software was employed for EE2 removal prediction.

### 3. RESULTS AND DISCUSSION

**3.1. Catalyst Screening.** To allow for a fair evaluation of the photocatalytic activity of several titania samples, experiments were performed at varying conditions, including the type of estrogen, catalyst to estrogen concentration ratio and the water matrix. As seen in Figure 1, Aerioxide P25 TiO<sub>2</sub> was more active irrespective of the experimental conditions in question, although its specific surface area is lower than that of the rest. For instance, 95% EE2 degradation was achieved after 10 min in UPW and 90 min in WW with Aerioxide P25, while the corresponding values for the second more active samples were 25 min in UPW (Kronos vlp 7100) and 120 min in WW (Hombikat UV 100). The degree of EE2 dark adsorption was 15% in UPW and 21% in WW with Aerioxide P25, 15 ± 5% in UPW, and 8 ± 3% in WW with the Kronos vlp family of photocatalysts, and 17% in UPW and 2% in WW with Hombikat UV 100. A similar trend occurred for E2, whose degradation in WW was complete after 90 min with Aerioxide P25 but it did not exceed 80% with any of the other catalysts.

The ability of semiconductor photocatalysis to oxidize organic species is due to the valence band holes photogenerated onto the titania surface, as well as the hydroxyl radicals produced from the reaction of holes with surface-bound water and hydroxyl anions. Moreover, the formation of peroxide radicals through reactions involving conduction band electrons, dissolved oxygen and protons cannot be excluded.<sup>21,22</sup>

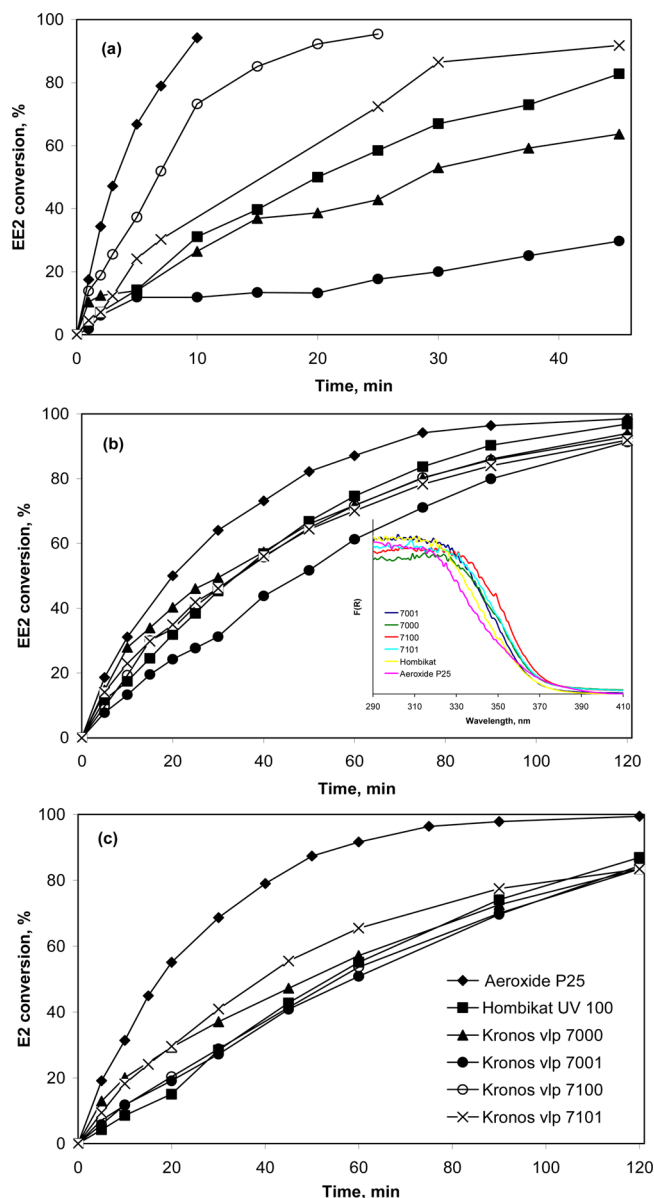


**Figure 1.** Relative activity of various titania samples (legends as in Figure 1c) for the degradation of (a) 300 µg/L EE2 in UPW with 50 mg/L TiO<sub>2</sub>; (b) 100 µg/L EE2 in WW with 250 mg/L TiO<sub>2</sub>; (c) 100 µg/L EE2 in WW with 250 mg/L TiO<sub>2</sub>. DRS of titania samples are given in the inset graph.

Hydroxyl radicals are considered as the primary oxidizing chemical species, acting not only on the surface but also in the solution phase.<sup>21</sup>

The superiority of Aerioxide P25 can be attributed<sup>23</sup> to the slower electron/hole recombination, which takes place on the catalyst surface compared to other TiO<sub>2</sub> samples. Another explanation ascribes its higher activity to its structure, which is a mixture of anatase and rutile; this mixture is more active than the individual pure crystalline phases.<sup>24</sup> It is also worth noting that the Kronos vlp family, which are carbon-doped TiO<sub>2</sub> samples, absorb in a slightly wider part of the electromagnetic spectrum according to the DRS shown in the inset of Figure 1b; nevertheless, they were less active than Aerioxide P25.

An additional experiment (not shown) was performed without catalyst at the conditions of Figure 1a, leading to just 7% EE2 removal after 10 min; this confirms that degradation is

predominantly due to the interaction between photon energy and the catalyst surface, rather than photolysis and/or photooxidation.

Further EE2 degradation experiments (not shown) were performed with Aeroxide P25 in UPW and WW under continuous aeration; the rationale behind this was to enhance electron trapping by dissolved oxygen, thus reducing the extent of electron/hole recombination, which is a major cause for reduced photocatalytic activity. Furthermore, oxygen is converted to superoxide radical anion, which can react with protons formed through water splitting to yield peroxide radicals. Air bubbling had no effect on the performance, possibly due to the fact that the concentration of oxygen inherently dissolved in the liquid was sufficient for electron scavenging. According to these findings, subsequent experiments were performed with Aeroxide P25  $\text{TiO}_2$  without gas sparging.

**3.2. Effect of Catalyst Loading.** The effect of  $\text{TiO}_2$  loading in the range 25–250 mg/L in UPW and 50–1500 mg/L in WW on EE2 degradation at 300 and 100  $\mu\text{g/L}$ , respectively was studied and the results are shown in Figure 2.

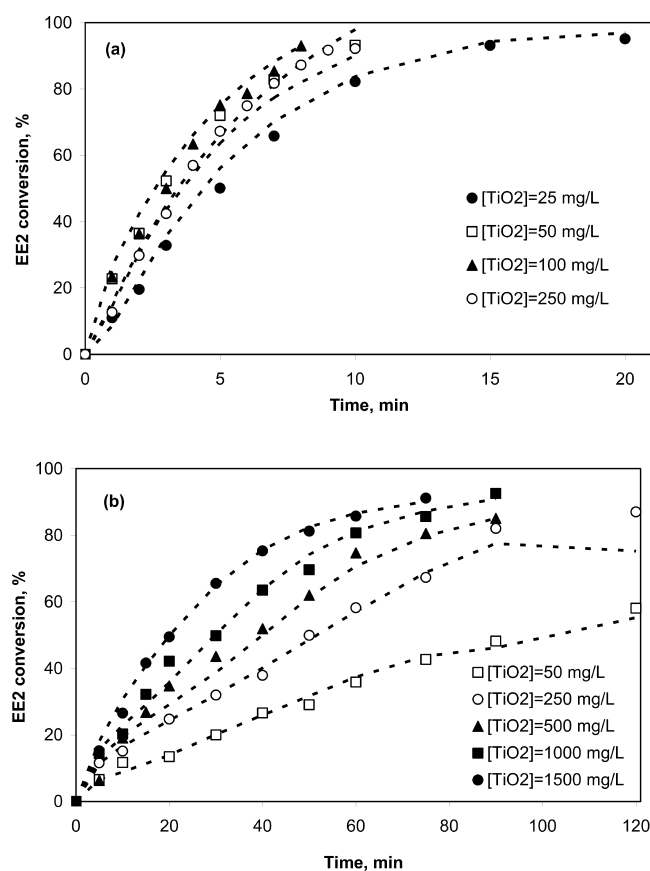


**Figure 2.** Effect of P25  $\text{TiO}_2$  loading on the degradation of (a) 300  $\mu\text{g/L}$  EE2 in UPW; (b) 100  $\mu\text{g/L}$  EE2 in WW. Symbols correspond to experimental data and dashed lines to ANN models.

An EE2 degradation of 93% in UPW was achieved after 15 min at 25 mg/L and 8–10 min at 50–250 mg/L catalyst, respectively. The effect of catalyst loading was more pronounced for the experiments in WW, where degradation was enhanced throughout the whole range of loadings studied. Interestingly, reactions in WW appear to be much slower than those in UPW and this is presumably associated with the effect

of water matrix species, as will be discussed in detail in section 3.4; for instance, 58% EE2 conversion was achieved after 120 min in WW at 50 mg/L catalyst (i.e., at a catalyst to EE2 concentration ratio of 1:2), while 95% conversion was achieved after just 20 min in UPW at 25 mg/L catalyst (i.e., at a far lower catalyst to EE2 concentration ratio of 1:12).

The increase in the photocatalytic activity with increasing catalyst loading indicates a heterogeneous catalytic regime, since the fraction of incident light absorbed by the semiconductor progressively increases in suspensions containing higher amounts of  $\text{TiO}_2$ .<sup>25</sup> Increasing catalyst loading apparently results in an increased number of catalyst active sites that are available for photocatalytic reactions and this occurs up to a point where all catalyst particles become fully illuminated.<sup>26</sup>

**3.3. Effect of Estrogen Concentration.** Figure 3 shows EE2 concentration–time profiles during photocatalytic oxida-

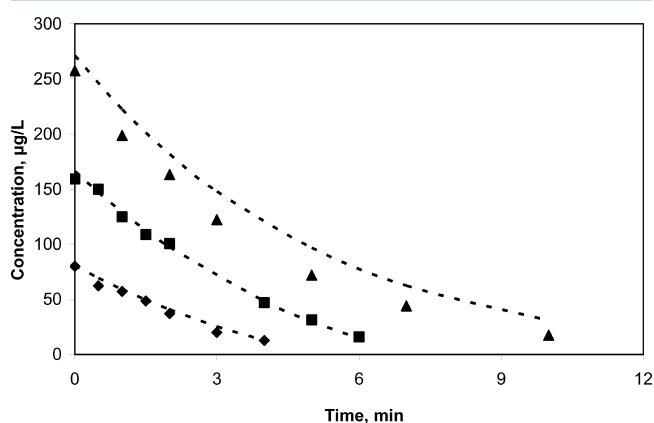


**Figure 3.** Effect of initial EE2 concentration on degradation in UPW with 50 mg/L P25  $\text{TiO}_2$ . Symbols correspond to experimental data and dashed lines to ANN models.

tion in UPW at 85, 160, and 300  $\mu\text{g/L}$  initial estrogen concentration (values at  $t = 0$  min correspond to the equilibrium concentration). Initial reaction rates,  $r_0$ , computed after 1 min of reaction take values of 22.8, 34.2, and 58.6  $\mu\text{g}/(\text{L}\cdot\text{min})$  at 85, 160, and 300  $\mu\text{g/L}$  EE2 concentration, respectively. The increase in reaction rate is almost proportional (although somewhat lower) to the respective concentration increase, which implies that the reaction rate approaches first order with respect to EE2 concentration.

In photocatalytic processes, substrate degradation can be described by the Langmuir–Hinshelwood (L–H) kinetic model;<sup>22,25</sup> that is,

$$r_0 = k_r \frac{KC_{\text{eq}}}{1 + KC_{\text{eq}}} \Leftrightarrow \frac{1}{r_0} = \frac{1}{k_r K C_{\text{eq}}} + \frac{1}{k_r} \quad (1)$$

where  $r_0$  is the initial reaction rate for EE2 photocatalytic degradation,  $C_{\text{eq}}$  is the equilibrium EE2 concentration,  $K$  is the adsorption constant of EE2 onto the catalyst surface, and  $k_r$  is the intrinsic reaction rate constant for EE2 degradation.

In the present experiments, it was found that adsorption of EE2 onto the catalyst surface in the dark was practically negligible (i.e., less than 5%). In such case and if  $KC_{\text{eq}} \ll 1$ , eq 1 can be written as follows:

$$r_0 = k_r KC_{\text{eq}} = k_{\text{app}} C_{\text{eq}} \quad (2)$$

where  $k_{app}$  is the apparent first order reaction rate constant for EE2 photocatalytic degradation, which incorporates the concentration of oxidizing species that, upon continuous irradiation at a fixed photon flux and  $\text{TiO}_2$  loading, are produced at a constant rate. In the present study, for the range of concentrations and experimental conditions in question, photocatalytic degradation of EE2 appears to follow near-first order kinetics.

**3.4. Effect of the Water Matrix.** The water matrix effect on 100  $\mu\text{g/L}$  EE2 degradation with 250  $\text{mg/L}$  Aeroxide P25 is demonstrated in Figure 4a. As seen, treatment efficiency

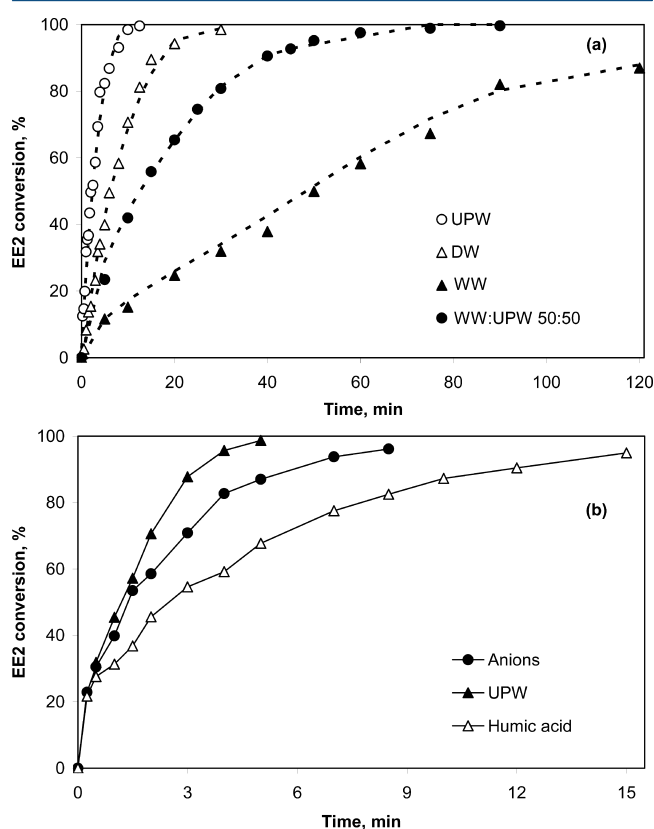


**Figure 4.** Degradation of 100  $\mu\text{g/L}$  EE2 with 250  $\text{mg/L}$  P25  $\text{TiO}_2$  in (a) various water matrices at their inherent pH; (b) UPW spiked with anions or humic acid at  $\text{pH} \approx 8.5$ . Symbols correspond to experimental data and dashed lines to ANN models.

decreases in the order:  $\text{UPW} > \text{DW} > \text{WW-UPW mixture} > \text{WW}$ . The apparent first order reaction rate constants can be computed from the slopes of  $\ln(C_0/C)$  versus time lines (not shown), as follows:  $367.1 \times 10^{-3}$  (0.974),  $137.7 \times 10^{-3}$  (0.989),  $60.2 \times 10^{-3}$  (0.996) and  $16.3 \times 10^{-3} \text{ min}^{-1}$  (0.966) with the numbers in brackets being the regression coefficients,  $r^2$ , of linear fitting.

Degradation in DW is as much as about 2.5 times slower than in UPW and this is presumably due to the presence of bicarbonates that behave as radical scavengers.<sup>27</sup> The fact that the two matrices have different pH values (i.e.,  $\sim 6$  for UPW and  $\sim 8$  for DW) is not expected to alter the ionization state of EE2 (and, consequently, its interaction with the catalyst surface), which will exist in its molecular form since it has a  $\text{pK}_a$  value of 10.2.<sup>28</sup> Nonetheless, changes in pH may affect the rate of reactive oxygen species formation and, consequently, degradation kinetics. To check for this, an additional experiment in UPW was performed raising solution pH to  $\sim 8.5$  and

the EE2 conversion–time profile is shown in Figure 4b; alkaline conditions seem to favor degradation with the reaction rate constant becoming  $656.8 \times 10^{-3} \text{ min}^{-1}$  (0.982).

The detrimental role of nontarget constituents typically found in environmental samples is evident comparing rates in UPW and WW. The latter contains chlorides and sulfates that react with hydroxyl radicals to form the respective radicals; although these may still oxidize EE2, their oxidation potential is lower than that of hydroxyl radicals.<sup>29</sup> Furthermore, it contains bicarbonates that are expected to act as radical scavengers. Besides the presence of inorganic species, the residual organic matter of WW, which is highly resistant to degradation by photochemical and other advanced oxidation processes,<sup>30,31</sup> competes with EE2 for the photogenerated oxidizing species. Given that (i) EE2 constitutes only about 1% of the organic content of the WW matrix (i.e., 80  $\mu\text{g/L}$  of carbon due to EE2 and 8.4  $\text{mg/L}$  due to WW), and (ii) photocatalytic oxidation is nonselective, most of hydroxyl radicals and other oxidizing species are likely to be wasted attacking the nontarget constituents of WW.

To gain a better insight of the role of the known nontarget constituents typically found in WW, experiments were performed in UPW spiked with either 15  $\text{mg/L}$  of humic acid or a mixture of anions containing 267  $\text{mg/L}$   $\text{NaHCO}_3$ , 283  $\text{mg/L}$   $\text{NaCl}$ , 80  $\text{mg/L}$   $\text{Na}_2\text{SO}_4$ , 51  $\text{mg/L}$   $\text{NaNO}_3$ , 55  $\text{mg/L}$   $\text{NaNO}_2$ , and 45  $\text{mg/L}$   $\text{NaH}_2\text{PO}_4 \cdot \text{H}_2\text{O}$ ; as seen in Figure 4b, the presence of humic acid or anions is detrimental to degradation with the respective rate constants being equal to 34% and 61% of the value in UPW. Interestingly though, the detrimental effect of the actual WW matrix is far more serious (e.g., the rate constant in WW is only 5% of that in UPW, as seen in Figure 4a); this implies that various unknown WW constituents (mainly organic compounds) are also responsible for decreased kinetics.

**3.5. Relative Reactivity of E1, E2, and EE2.** In further experiments, a mixture of 200  $\mu\text{g/L}$  E1, 100  $\mu\text{g/L}$  E2, and 100  $\mu\text{g/L}$  EE2 was subject to photocatalytic oxidation in UPW and WW, while the respective single-component systems were also tested. It should be noted here that estrogen concentrations were chosen in such a way to represent their relative contribution in environmental matrices, i.e., E1 concentration is usually greater than the other two.<sup>4,5</sup> The results, in terms of conversion and initial rates, are shown in Figure 5.

Reactivity in UPW is expectedly greater than in WW and decreases in the order  $\text{E1} > \text{E2} \approx \text{EE2}$ ; nevertheless, differences are not great given the structural similarities of the three estrogens. A similar order was found by Li Puma et al.<sup>8</sup> who studied the UV-A/Aeroxide P25 degradation of an equimolar mixture of various estrogens including E1, E2, and EE2. Degradation in the mixture is slower than in single-component systems, which indicates a competition among the estrogens (as well as the nontarget constituents in WW) for the oxidizing species. The overall initial rate of the mixture is 83.6  $\mu\text{g}/(\text{L} \cdot \text{min})$  in UPW and 12.3  $\mu\text{g}/(\text{L} \cdot \text{min})$  in WW, while the respective values of the single E1 system are 66.6 and 9.5  $\mu\text{g}/(\text{L} \cdot \text{min})$ . Ignoring the (relatively low) differences in estrogen reactivity, one can see that doubling estrogen concentration from 200 to 400  $\mu\text{g/L}$  results in only about 30% rate increase in either matrix. Following from the discussion in section 3.3, this denotes a transition from first to lower order kinetics regarding estrogen concentration and it is attributed to the fact that the oxidizing species become the limiting reactant as estrogen concentration increases.

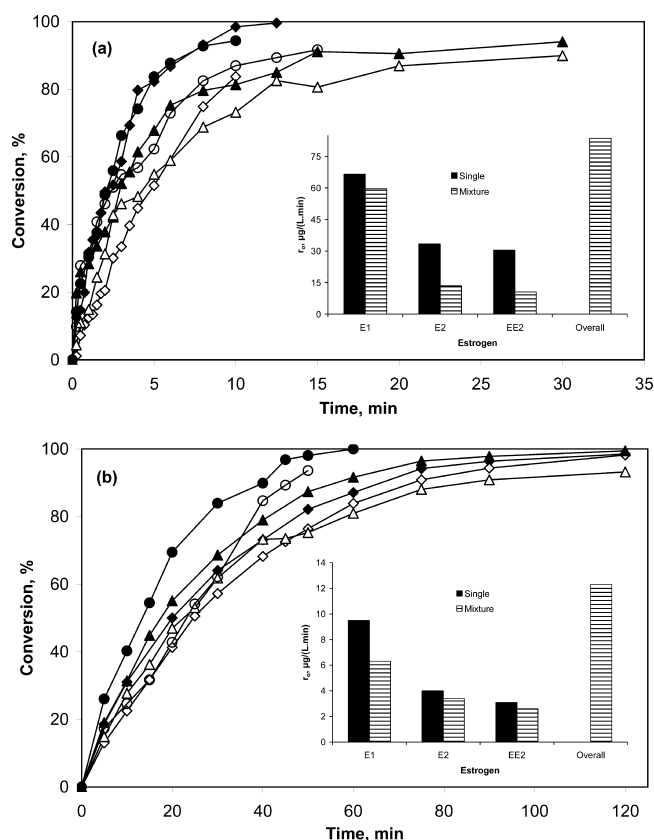


**Figure 5.** Degradation of E1 (●,○), E2 (▲,△), EE2 (◆,◇) in single component systems (filled symbols) and mixtures (open symbols) in (a) UPW; (b) WW with 250 mg/L P25  $\text{TiO}_2$ .  $[\text{E1}]_0 = 200 \mu\text{g/L}$ ,  $[\text{E2}]_0 = [\text{EE2}]_0 = 100 \mu\text{g/L}$ . Inset graphs show rates after 1 min in UPW and 5 min in WW.

**3.6. Removal of Estrogenicity.** Figure 6 shows changes of estrogenicity as a function of treatment time for the mixture of

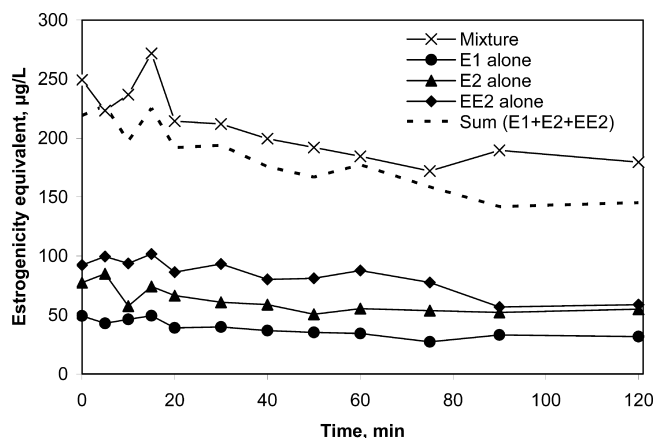


**Figure 6.** Change of estrogenicity (as assessed by the YES test) during the photocatalytic degradation of E1, E2, EE2 in single component systems and mixture in WW with 250 mg/L P25  $\text{TiO}_2$ .  $[\text{E1}]_0 = 200 \mu\text{g/L}$ ,  $[\text{E2}]_0 = [\text{EE2}]_0 = 100 \mu\text{g/L}$ .

E1, E2, and EE2, as well as the respective single-component systems in WW. The estrogenicity equivalent (EEQ) of 200  $\mu\text{g/L}$  E1, 100  $\mu\text{g/L}$  E2, and 100  $\mu\text{g/L}$  EE2 is 49.2, 77.4, and 92.4  $\mu\text{g/L}$ , respectively, thus showing that EE2 is 20% more potent, while E1 is 68% less potent than E2 (taking into

account concentration differences between E1 and E2). These results are in very good agreement with the E2 equivalency factors reported by Beck et al.<sup>1</sup> with EE2 being 25% more potent and E1 75% less potent than E2. The EEQ of the mixture is 249.3  $\mu\text{g/L}$ , which is nearly equal to the sum of EEQs of the individual estrogens.

It is notable that even after prolonged photocatalytic treatment, all matrices retained most of their initial estrogenicity. Although complete estrogen degradation was achieved after 120 min of reaction (Figure 5b), this was accompanied by partial estrogenicity removal, which never exceeded 36% (Figure 6). Interestingly, the estrogenicity profile of the mixture resembles that of the single-component systems and matches closely the sum of the profiles of the individual components (given by the dashed line in Figure 6). These results clearly show that the photocatalytic transformation of E1, E2, and EE2, as well as the WW organic matter generates certain stable byproducts that are estrogenically potent and responsible for most of the remaining estrogenicity; this cannot be attributed to the matrix itself, since its inherent EEQ (i.e., prior to spiking) was just 5.6  $\mu\text{g/L}$ . We have recently reported similar discrepancies between estrogen and estrogenicity removal during treatment by photo-Fenton oxidation<sup>32</sup> and sonochemical radiation.<sup>33</sup> Bistan et al.,<sup>34</sup> who studied the degradation of xeno-estrogen bisphenol A in UPW with Aeroxide P25 under UV-A radiation, reported that complete estrogen removal after 360 min of reaction was accompanied by only 23% estrogenicity reduction; this was assigned to the formation of more estrogenic byproducts.

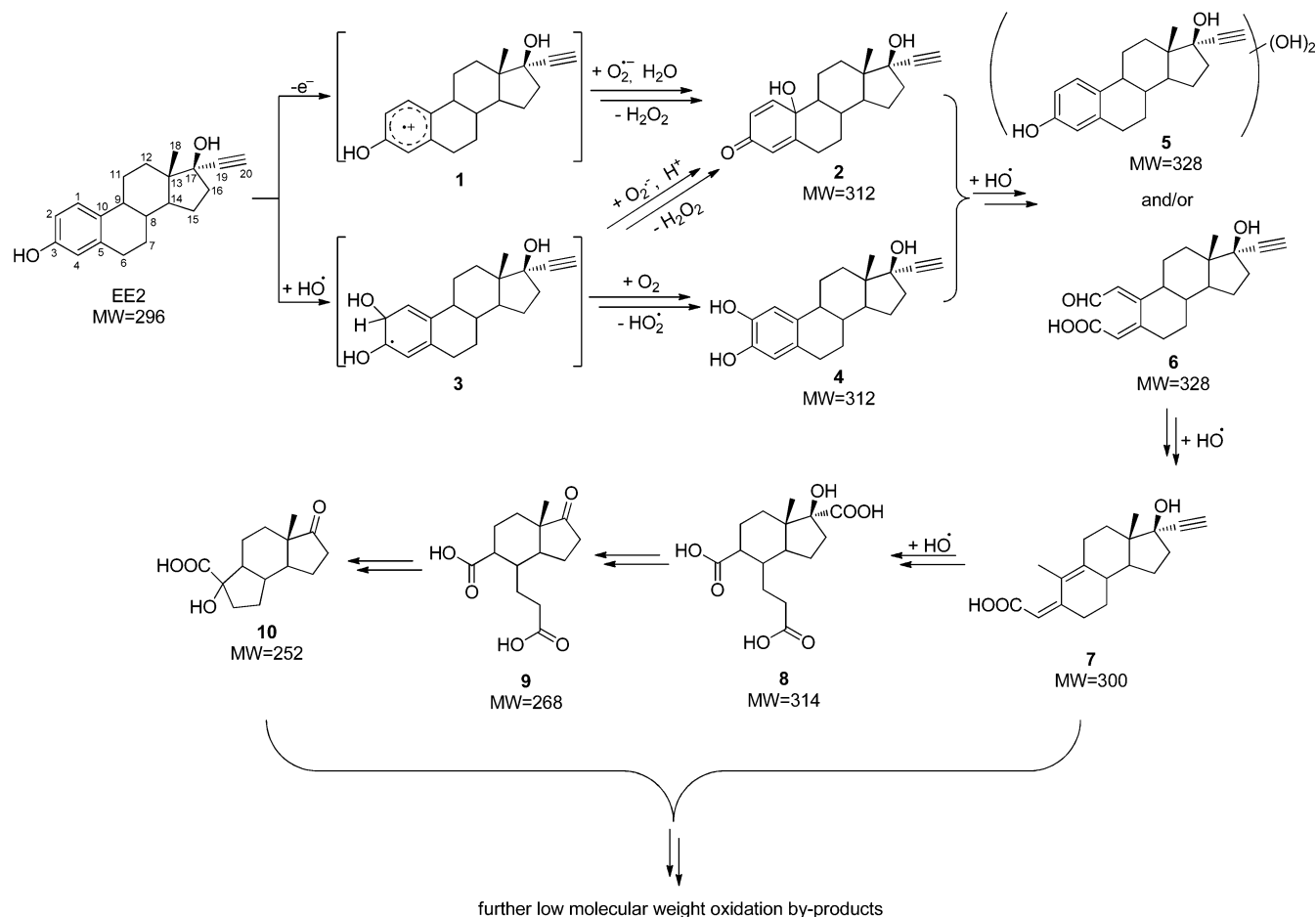
**3.7. Identification of EE2 Photocatalytic Oxidation Byproducts in UPW.** An attempt was made to determine major oxidation byproducts formed during the photocatalytic oxidation of EE2 in UPW. EE2 was chosen because it exhibits higher estrogenic activity than E2 and E1, as can be seen in Figure 6. EE2 at 800  $\mu\text{g/L}$  initial concentration was prepared in UPW, then slurried with 50 mg/L Aeroxide P25  $\text{TiO}_2$  and illuminated for 60 min. An increased estrogen concentration was employed to facilitate the determination of reaction byproducts. Several samples were drawn at various treatment times, centrifuged to remove catalyst particles, and then analyzed by LC-MS/MS. Several major product ions were found at  $m/z$  329,  $m/z$  315,  $m/z$  313,  $m/z$  301,  $m/z$  268, and  $m/z$  253, as well as other ions corresponding to lower molecular weight compounds. Ionization of the parent compound as well as of the degradation byproducts was performed in the positive ionization mode; therefore all the above ions correspond to the protonated molecular ion,  $[\text{M} + \text{H}]^+$ .

On the basis of the above results, as well as on previous studies published by our research group<sup>35</sup> and other researchers,<sup>9,36–47</sup> we tentatively identified several degradation byproducts of the photocatalytic oxidation of EE2 in UPW; these can be seen in Schematic 2, alongside the proposed reaction pathways.

There are two principal oxidation mechanisms of EE2 under photocatalytic conditions, namely (i) oxidation by the valence band holes ( $h^+$ ), and (ii) direct hydroxyl radical attack. Oxidation by the valence band holes is accomplished by electron abstraction from the EE2 molecule, resulting in the formation of the intermediate cationic radical **1** (Schematic 2). In a recent study performed by Singhal and co-workers,<sup>37</sup> frontier electron density values for the different carbon atoms of EE2 were calculated. It was found that the electron density



Scheme 2. The Proposed Reaction Pathway for the Photocatalytic Degradation of EE2 in UPW



was higher for the carbon atoms at positions 3 and 10 of the aromatic ring of EE2 (for the numbering of carbon atoms see Schematic 2), with carbon at position 10 having the highest value of electron density of all the atoms in EE2. This finding is in perfect agreement with the frontier electron density calculation performed by Fujishima and co-workers<sup>38</sup> a decade ago on the structurally similar E2 molecule (Schematic 1), which showed that carbon atoms at positions 3 and 10 of the aromatic ring have higher electron density than other carbon atoms in the molecule of E2, with carbon at position 10 having the highest value. These calculations indicate that the most probable sites at which an electron would be abstracted by a hole are the carbon atoms at positions 3 and 10 of the aromatic ring of EE2. Given that there is relatively little steric hindrance to attack by electrophiles at the aromatic ring of EE2, it can be anticipated that the carbon atom at position 10 should be the most favorable site for attack.

Further attack of superoxide radicals,  $O_2^{\cdot-}$ , to cationic radical **1** at the position 10 of the aromatic ring results in a multistep reaction pathway to 17 $\alpha$ -ethynyl-1,4-estradiene-10 $\epsilon$ ,17 $\beta$ -diol-3-one **2**.<sup>38</sup> It is worth mentioning that Singhal and co-workers,<sup>37</sup> using liquid chromatography-time-of-flight-mass spectroscopy (LC-ToF-MS) and nuclear magnetic resonance (NMR) spectroscopy, confirmed that the initial oxidation products of the reaction of EE2 with iron complexes of tetra-amido macrocyclic ligands ( $Fe^{III}$ -TAMLs) in the presence of  $H_2O_2$  ( $Fe^{III}$ -TAML/ $H_2O_2$ ) were the 10 $\alpha$  and 10 $\beta$  epimers of 17 $\alpha$ -ethynyl-1,4-estradiene-10 $\epsilon$ ,17 $\beta$ -diol-3-one **2**. In addition, the

same group reported that compound **2** is associated with increased estrogenic activity compared to EE2.<sup>37</sup> Moreover, compound **2** has been identified as an intermediate degradation byproduct during ozonation of EE2,<sup>39</sup> while the corresponding 10 $\epsilon$ ,17 $\beta$ -dihydroxy-1,4-estradiene-3-one (DEO) has been identified as an intermediate degradation byproduct of E2 during various advanced oxidation processes, such as  $TiO_2$  photocatalysis,<sup>38,40</sup> ozonation,<sup>41,42</sup> heterogeneous photo-Fenton oxidation,<sup>43</sup> and visible light dye-photosensitized degradation.<sup>44</sup>

On the other hand, oxidation of EE2 may be initiated by the addition of the photocatalytically generated hydroxyl radicals to the EE2 molecule. There are three possible sites on the EE2 molecule for hydroxyl radicals attack, namely (i) the aromatic ring, (ii) the aliphatic rings, and (iii) the ethynyl moiety (i.e., the triple bond) of EE2.<sup>45</sup> It has been reported that the kinetic ratio among the three pathways is expected to be 10:8:5 for paths i/ii/iii.<sup>45</sup> The frontier electron density calculations on E2 showed that the most probable sites of hydroxyl radicals attack are the carbon atoms at positions 2 and 5 of the aromatic ring, with the carbon atom at position 2 being the most probable site of attack.<sup>38</sup> If the addition of hydroxyl radicals takes place at the carbon atom in position 2 of the aromatic ring, the intermediate radical **3** could be formed, which after a subsequent reaction with  $O_2$  could lead to the corresponding 2-OH EE2 **4**, as shown in Schematic 2. In addition, compound **2** could be also formed from the intermediate radical **3**, in a multistep reaction mechanism, as shown in Schematic 2.<sup>38</sup> However, other hydroxylated intermediate oxidation byproducts may be formed



from the addition of hydroxyl radicals at other positions of the aromatic or aliphatic rings of EE2.<sup>36</sup> Nevertheless, it is worth mentioning that compounds **2** and **4** are the most frequently identified oxidation byproducts of E2 and EE2 using various advanced oxidation processes.<sup>36</sup> Therefore, the ion at  $m/z$  313 most probably corresponds to compound **2** and/or to compound **4**.

Further hydroxyl radical attack to compounds **2** and/or **4** could yield compound **5**, in which two hydroxyl groups have been added to the EE2 molecule, and/or compound **6**, in which the aromatic ring of EE2 has been cleaved. Such a ring-cleavage oxidation byproduct has been reported in the TiO<sub>2</sub> photocatalytic oxidation of EE2.<sup>9</sup> Therefore, compounds **5** and/or **6** most probably correspond to the ion found at  $m/z$  329. Further oxidation of the above-mentioned intermediate byproducts could result in the formation of compounds **7**, **8**, **9**, and **10**,<sup>9,36,46</sup> which eventually lead to low molecular weight compounds, corresponding to aliphatic carboxylic acids and other ring-cleavage compounds. Finally, regarding the relationship between degradation byproducts and the remaining estrogenicity, it should be emphasized that it is very difficult to identify which oxidation byproducts are mainly responsible for the remaining estrogenicity after the photocatalytic treatment.

**3.8. Modeling of EE2 Removal.** The optimum number of neurons required to build an ANN can be derived minimizing the mean square error, MSE, which is defined as follows:

$$\text{MSE} = \frac{\sum_{i=1}^N (y_{i,\text{pred}} - y_{i,\text{expt}})^2}{N} \quad (3)$$

where  $y_{i,\text{pred}}$  and  $y_{i,\text{expt}}$  are the predicted and experimental values of the dependent variable, respectively, and  $N$  is the number of data. To do so, a series of topologies were employed, in which the number of neurons was varied between 1 and 15. Each topology was repeated five times at least to avoid random correlation due to the random initialization of the weights. As seen in Figure 7, MSE is  $2.57 \times 10^{-2}$  for just one neuron, and it is minimized to  $7.74 \times 10^{-4}$  for eight neurons; the resulting ANN is schematically illustrated in Figure 8.

Figure 9 shows a comparison between the measured EE2 conversion and the predicted values to test the precision of the ANN model; there are two lines corresponding to (i) the perfect fit,  $y = x$  (i.e., experimental and predicted values would be identical), and (ii) the best linear fit,  $y = 0.994x + 0.0059$ ,

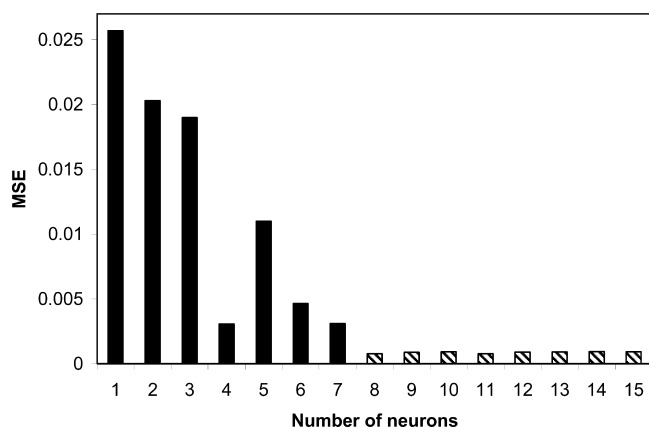


Figure 7. Optimization of number of neurons in relation to MSE.

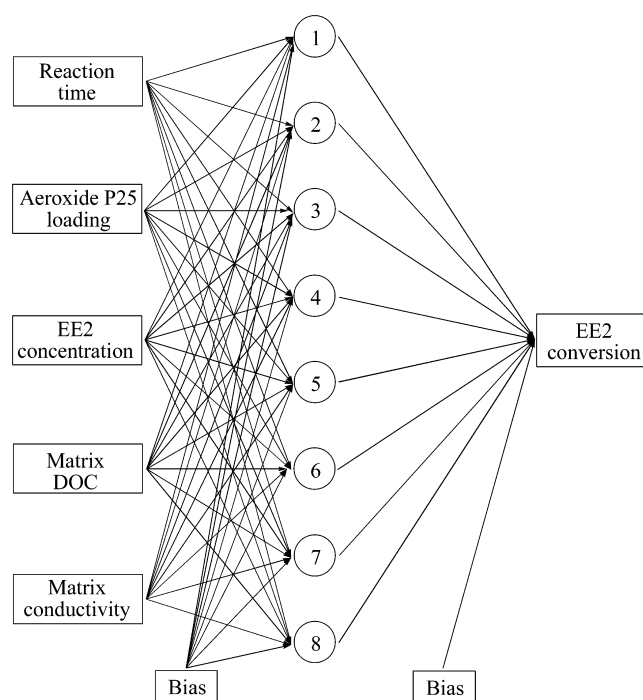


Figure 8. Structure of the optimized ANN used in this work.

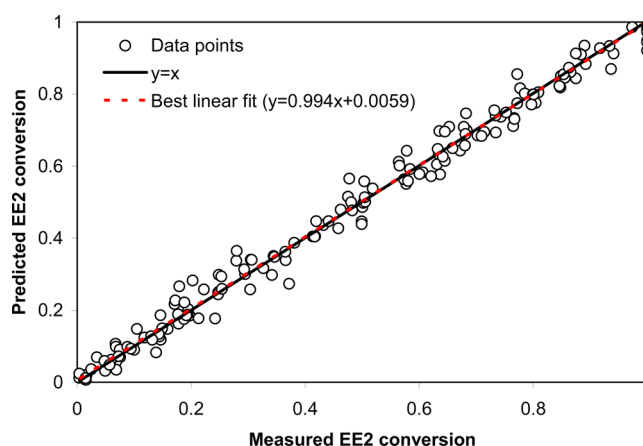


Figure 9. Comparison between measured and predicted values of the dependent variable.

obtained with regression analysis. The regression coefficient is 0.988, thus implying a very good fit, which is demonstrated in Figures 2–4 for representative experiments. Apparent rate constants were also computed from the measured and predicted conversion profiles and the results are shown in Figure 10. In most cases, the ratio between experimental and modeled rate constants approaches unity, thus verifying the good fit.

Finally, the relative significance of the input variables was evaluated using the neural weight matrix and the following equation proposed by Garson:<sup>48</sup>

$$I_j = \frac{\sum_{m=1}^{N_h} ((|w_{jm}^{ih}| / \sum_{k=1}^{N_i} |w_{km}^{ih}|) |w_{mn}^{ho}|)}{\sum_{k=1}^{N_i} \{ \sum_{m=1}^{N_h} (|w_{km}^{ih}| / \sum_{k=1}^{N_i} |w_{km}^{ih}|) |w_{mn}^{ho}| \}} \quad (4)$$

where  $I_j$  is the relative significance of the  $j$ th input variable on the output variable,  $N_i$  and  $N_h$  are the numbers of input and hidden neurons, respectively, and  $w$  is the connection weight.

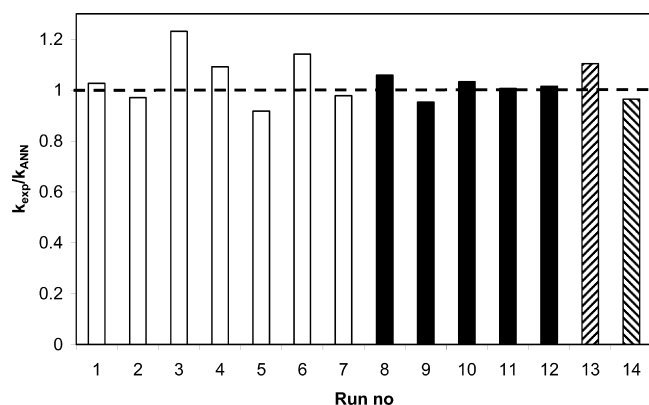


**Figure 10.** Comparison between experimental and modeled apparent rate constants for EE2 degradation in UPW (runs 1–7), WW (runs 8–12), WW:UPW mixture (run 13), and DW (run 14). Other conditions as in Figures 3 (runs 1–3), 2a (runs 4–7), 2b (runs 8–12), and 4a (runs 13–14).

The subscripts k, m, and n refer to input, hidden, and output neurons, respectively, while the superscripts i, h, and o refer to input, hidden, and output layers, respectively. The weight matrix of the ANN model in question is given in Table 3, while the relative significance of the input variables derived from eq 4 is given in Table 2. For the range of experimental conditions in question, the reaction time is the single most influential variable (45.3%) followed by the water matrix characteristics (26.7% collectively).

#### 4. CONCLUSIONS

The conclusions drawn from the present study can be summarized as follows:

(1) Solar-driven semiconductor photocatalysis is an efficient method for the degradation of estrogen hormones in environmental samples. Commercially available Aeroxide P25 TiO<sub>2</sub> (75:25 anatase/rutile mixture) was substantially more active than other titania samples tested in this work.

(2) Variables that may decisively affect treatment performance can be classified into two groups, namely, (i) the actual operating conditions including treatment time, the type and concentration of catalyst, the type and concentration of estrogen, air sparging, etc., and (ii) the complexity of the water matrix with respect to its inorganic and organic composition. Although working with model solutions may still provide some useful information, actual treatment conditions can realistically be represented employing environmentally relevant matrices.

(3) The complete degradation of individual estrogenic compounds is not necessarily accompanied by the removal of associated estrogenicity; this strengthens further the need of (i) working with actual rather than model matrices and (ii) applying specific (bio)assays beyond conventional analytical protocols. A complex reaction network occurs in the photocatalytic oxidation of EE2 involving the formation of several oxidation byproducts.

(4) A 5-8-1 artificial neural network was optimized, tested, and validated for the photocatalytic degradation of 17 $\alpha$ -ethynylestradiol. The resulting model comprised five variables, that is, reaction time, catalyst loading, estrogen concentration, matrix DOC, and conductivity with reaction time being the single most important one. For the set of operating variables in question, degradation profiles could be predicted successfully, thus making ANN a useful tool in modeling water treatment processes.

#### AUTHOR INFORMATION

##### Corresponding Author

\*E-mail: nikos.xekoukoulotaki@enveng.tuc.gr. Tel.: +302821037772. Fax: +302821037848.

##### Notes

The authors declare no competing financial interest.

#### ACKNOWLEDGMENTS

The authors are grateful to the Cyprus Research Promotion Foundation for funding this research project (Research Project: Estrogens, PROEM/0308/06). Thanks are due to (i) Dr. E. Routledge (Brunel University, UK) for kindly supplying yeasts for the YES bioassay, and (ii) Dr. D. Kondarides (University of Patras, Greece) for DRS characterization. NIREAS is cofunded by the European Regional Development Fund and the Republic of Cyprus through the Research Promotion Foundation (Project NEA ΥΠΟΔΟΜΗ/ΣΤΡΑΤΗΓ/03/0308/09).

#### REFERENCES

- Beck, I. C.; Bruhn, R.; Gandrass, J. Analysis of estrogenic activity in coastal surface waters of the Baltic Sea using the yeast estrogen screen. *Chemosphere* **2006**, *63*, 1870–1878.
- Rizzo, L. Bioassays as a tool for evaluating advanced oxidation processes in water and wastewater treatment. *Water Res.* **2011**, *45*, 4311–4340.
- Desbrow, C.; Routledge, E. J.; Brighty, G. C.; Sumpter, J. P.; Waldock, M. Identification of estrogenic chemicals in STW effluent. 1. Chemical fractionation and in vitro biological screening. *Environ. Sci. Technol.* **1998**, *32*, 1549–1558.
- Servos, M. R.; Bennie, D. T.; Burnison, B. K.; Jurkovic, A.; McInnis, R.; Neheli, T.; Schnell, A.; Seto, P.; Smyth, S. A.; Ternes, T. A. Distribution of estrogens, 17 $\beta$ -estradiol and estrone, in Canadian

**Table 3.** Weight Matrix of the 5-8-1 ANN

neuron	input					output EE2 conversion
	reaction time	Aeroxide P25 loading	EE2 concentration	matrix DOC	matrix conductivity	
1	−1.58521	−2.9607500	−0.141804569	1.210735075	−2.412070098	−4.220967728
2	−0.70142	−0.9751351	−0.606856204	−0.303350637	1.481520134	3.637533217
3	−2.41468	−0.9199706	0.819532714	−0.104235594	−0.573431381	−1.227168256
4	−7.12719	0.22811353	−0.144310913	0.334309838	−1.076031464	7.012272258
5	−1.95509	0.29677417	0.63801784	1.766716111	1.313216297	1.768131515
6	0.34568	−1.7879048	−0.51776237	−0.351934376	−0.914874403	5.609020525
7	−1.86343	−0.5475625	0.245566838	0.53293257	0.067701549	2.222889876
8	−1.47062	−1.9603607	0.941887007	−1.526882584	0.534614819	2.019490706

municipal wastewater treatment plants. *Sci. Total Environ.* **2005**, 336, 155–170.

(5) Chang, H.; Wan, Y.; Wu, S.; Fan, Z.; Hu, J. Occurrence of androgens and progestogens in wastewater treatment plants and receiving river waters: Comparison to estrogens. *Water Res.* **2011**, 45, 732–740.

(6) Silva, C. P.; Otero, M.; Esteves, V. Processes for the elimination of estrogenic steroid hormones from water: A review. *Environ. Pollut.* **2012**, 165, 38–58.

(7) Zhang, Y.; Zhou, J. L.; Ning, B. Photodegradation of estrone and 17 $\beta$ -estradiol in water. *Water Res.* **2007**, 41, 19–26.

(8) Li Puma, G.; Puddu, V.; Tsang, H. K.; Gora, A.; Toepfer, B. Photocatalytic oxidation of multicomponent mixtures of estrogens (estrone (E1), 17 $\beta$ -estradiol (E2), 17 $\alpha$ -ethynylestradiol (EE2) and estriol (E3)) under UVA and UVC radiation: Photon absorption, quantum yields and rate constants independent of photon absorption. *Appl. Catal. B-Environ.* **2010**, 99, 388–397.

(9) Sun, W.; Li, S.; Mai, J.; Ni, J. Initial photocatalytic degradation intermediates/pathways of 17 $\alpha$ -ethynylestradiol: Effect of pH and methanol. *Chemosphere* **2010**, 81, 92–99.

(10) Karpova, T.; Preis, S.; Kallas, J. Selective photocatalytic oxidation of steroid estrogens in water treatment: Urea as co-pollutant. *J. Hazard. Mater.* **2007**, 146, 465–471.

(11) Chowdhury, R. R.; Charpentier, P.; Ray, M. B. Photodegradation of Estrone in Solar Irradiation. *Ind. Eng. Chem. Res.* **2010**, 49, 6923–6930.

(12) Chowdhury, R. R.; Charpentier, P. A.; Ray, M. B. Photodegradation of 17 $\beta$ -estradiol in aquatic solution under solar irradiation: Kinetics and influencing water parameters. *J. Photochem. Photobiol. A-Chem.* **2011**, 219, 67–75.

(13) Khataee, A. R.; Kasiri, M. B. Artificial neural networks modeling of contaminated water treatment processes by homogeneous and heterogeneous nanocatalysis. *J. Mol. Catal. A-Chem.* **2010**, 331, 86–100.

(14) Calza, P.; Sakkas, V. A.; Villioti, A.; Massolino, C.; Boti, V.; Pelizzetti, E.; Albanis, T. Multivariate experimental design for the photocatalytic degradation of imipramine: Determination of the reaction pathway and identification of intermediate products. *Appl. Catal. B-Environ.* **2008**, 84, 379–388.

(15) Duran, A.; Monteagudo, J. M. Solar photocatalytic degradation of reactive blue 4 using a Fresnel lens. *Water Res.* **2007**, 41, 690–698.

(16) Monteagudo, J. M.; Duran, A.; Guerra, J.; Garcia-Pena, F.; Coca, P. Solar TiO<sub>2</sub>-assisted photocatalytic degradation of IGCC power station effluents using a Fresnel lens. *Chemosphere* **2008**, 71, 161–167.

(17) Clesceri, L. S.; Greenberg, A. E.; Eaton, A. D. *Standard Methods for the Examination of Water and Wastewater*, 20th ed.; American Public Health Association: Washington, DC, USA, 1999.

(18) Willett, K. L.; Hites, R. A. Chemical actinometry: Using *o*-nitrobenzaldehyde to measure light intensity in photochemical experiments. *J. Chem. Educ.* **2000**, 77, 900–902.

(19) Galbavy, E. S.; Ram, K.; Anastasio, C. 2-Nitrobenzaldehyde as a chemical actinometer for solution and ice photochemistry. *J. Photochem. Photobiol. A-Chem.* **2010**, 209, 186–192.

(20) Routledge, E. J.; Sumpter, J. P. Estrogenic activity of surfactants and some of their degradation products assessed using a recombinant yeast screen. *Environ. Toxicol. Chem.* **1996**, 15, 241–248.

(21) Turchi, C. S.; Ollis, D. F. Photocatalytic degradation of organic water contaminants: Mechanisms involving hydroxyl radical attack. *J. Catal.* **1990**, 122, 178–192.

(22) Hoffmann, M. R.; Martin, S. T.; Choi, W.; Bahnemann, D. W. Environmental applications of semiconductor photocatalysis. *Chem. Rev.* **1995**, 95, 69–96.

(23) Martin, S. T.; Herrmann, H.; Choi, W.; Hoffmann, M. R. Time-resolved microwave conductivity. Part 1. TiO<sub>2</sub> photoreactivity and size quantization. *J. Chem. Soc. Faraday Trans.* **1994**, 90, 3315–3322.

(24) Bickley, R. I.; Gonzalez-Carreno, T.; Lees, J. S.; Palmisano, L.; Tilley, R. J. D. A structural investigation of titanium dioxide photocatalysts. *J. Solid State Chem.* **1991**, 92, 178–190.

(25) Herrmann, J.-M. Photocatalysis fundamentals revisited to avoid several misconceptions. *Appl. Catal. B-Environ.* **2010**, 99, 461–468.

(26) Yang, L.; Yu, L. E.; Ray, M. B. Degradation of paracetamol in aqueous solutions by TiO<sub>2</sub> photocatalysis. *Water Res.* **2008**, 42, 3480–3488.

(27) Vione, D.; Maddigapu, P. R.; de Laurentis, E.; Minella, M.; Pazzi, M.; Maurino, V.; Minero, C.; Kouras, S.; Richard, C. Modelling the photochemical fate of ibuprofen in surface waters. *Water Res.* **2011**, 45, 6725–6736.

(28) Fu, H.; Suri, R. P. S.; Chimchirian, R. F.; Helmig, E.; Constable, R. Ultrasound-induced destruction of low levels of estrogen hormones in aqueous solutions. *Environ. Sci. Technol.* **2007**, 41, 5869–5874.

(29) Poulis, I.; Kyriacou, G. Photocatalytic degradation of *p*-coumaric acid over TiO<sub>2</sub> suspensions. *Environ. Technol.* **2002**, 23, 179–187.

(30) Dialynas, E.; Mantzavinos, D.; Diamadopoulos, E. Advanced treatment of the reverse osmosis concentrate produced during reclamation of municipal wastewater. *Water Res.* **2008**, 42, 4603–4608.

(31) Li, W.; Nanaboina, V.; Zhou, Q.; Korshin, G. V. Effects of Fenton treatment on the properties of effluent organic matter and their relationships with the degradation of pharmaceuticals and personal care products. *Water Res.* **2012**, 46, 403–412.

(32) Frontistis, Z.; Xekoukoulotakis, N. P.; Hapeshi, E.; Venieri, D.; Fatta-Kassinos, D.; Mantzavinos, D. Fast degradation of estrogen hormones in environmental matrices by photo-Fenton oxidation under simulated solar radiation. *Chem. Eng. J.* **2011**, 178, 175–182.

(33) Frontistis, Z.; Mantzavinos, D. Sonodegradation of 17 $\alpha$ -ethynylestradiol in environmentally relevant matrices: Laboratory-scale kinetic studies. *Ultrason. Sonochem.* **2012**, 19, 77–84.

(34) Bistan, M.; Tisler, T.; Pintar, A. Catalytic and photocatalytic oxidation of aqueous bisphenol A solutions: Removal, toxicity, and estrogenicity. *Ind. Eng. Chem. Res.* **2012**, 51, 8826–8834.

(35) Frontistis, Z.; Daskalaki, V. M.; Hapeshi, E.; Drosou, C.; Fatta-Kassinos, D.; Xekoukoulotakis, N. P.; Mantzavinos, D. Photocatalytic (UV-A/TiO<sub>2</sub>) degradation of 17 $\alpha$ -ethynylestradiol in environmental matrices: Experimental studies and artificial neural network modelling. *J. Photochem. Photobiol. A-Chem.* **2012**, 240, 33–41.

(36) Pereira, R. O.; Postigo, C.; de Alda, M. L.; Daniel, L. A.; Barceló, D. Removal of estrogens through water disinfection processes and formation of by-products. *Chemosphere* **2011**, 82, 789–799.

(37) Chen, J. L.; Ravindran, S.; Swift, S.; Wright, L. J.; Singhal, N. Catalytic oxidative degradation of 17 $\alpha$ -ethynylestradiol by Fe<sup>III</sup>-TAML/H<sub>2</sub>O<sub>2</sub>: Estrogenicities of the products of partial, and extensive oxidation. *Water Res.* **2012**, 46, 6309–6318.

(38) Ohko, Y.; Iuchi, K.; Niwa, C.; Tatsuma, T.; Nakashima, T.; Iguchi, T.; Kubota, Y.; Fujishima, A. 17 $\beta$ -Estradiol degradation by TiO<sub>2</sub> photocatalysis as a means of reducing estrogenic activity. *Environ. Sci. Technol.* **2002**, 36, 4175–4181.

(39) Zhang, X.; Chen, P.; Wu, F.; Deng, N.; Liu, J.; Fang, T. Degradation of 17 $\alpha$ -ethynylestradiol in aqueous solution by ozonation. *J. Hazard. Mater.* **2006**, B133, 291–298.

(40) Mai, J.; Sun, W.; Xiong, L.; Liu, Y.; Ni, J. Titanium dioxide mediated photocatalytic degradation of 17 $\beta$ -estradiol in aqueous solution. *Chemosphere* **2008**, 73, 600–606.

(41) de Oliveria Pereira, R.; de Alda, M. L.; Joglar, J.; Daniel, L. A.; Barceló, D. Identification of new ozonation disinfection byproducts of 17 $\beta$ -estradiol and estrone in water. *Chemosphere* **2011**, 84, 1535–1541.

(42) Bila, D.; Montalvão, A. F.; de A. Azevedo, D.; Dezotti, M. Estrogenic activity removal of 17 $\beta$ -estradiol by ozonation and identification of by-products. *Chemosphere* **2007**, 69, 736–746.

(43) Zhao, Y.; Hu, J.; Jin, W. Transformation of oxidation products and reduction of estrogenic activity of 17 $\beta$ -estradiol by a heterogeneous photo-Fenton reaction. *Environ. Sci. Technol.* **2008**, 42, 5277–5284.

(44) Diaz, M.; Luiz, M.; Alegretti, P.; Furlong, J.; Amat-Guerri, F.; Massad, W.; Criado, S.; Garcia, N. A. Visible-light-mediated photo-degradation of 17 $\beta$ -estradiol: Kinetics, mechanism and photoproducts. *J. Photochem. Photobiol. A: Chem.* **2009**, 202, 221–227.

- (45) Lee, Y.; Escher, B. I.; von Gunten, U. Efficient removal of estrogenic activity during oxidative treatment of waters containing steroid estrogens. *Environ. Sci. Technol.* **2008**, *42*, 6333–6339.
- (46) Huber, M. M.; Ternes, T. A.; von Gunten, U. Removal of estrogenic activity and formation of oxidation products during ozonation of 17 $\alpha$ -ethinylestradiol. *Environ. Sci. Technol.* **2004**, *38*, 5177–5186.
- (47) Jiang, J.; Pang, S.-Y.; Jun, Ma, J.; Liu, H. Oxidation of phenolic endocrine disrupting chemicals by potassium permanganate in synthetic and real waters. *Environ. Sci. Technol.* **2012**, *46*, 1774–1781.
- (48) Garson, G. D. Interpreting neural-network connection weights. *Artif. Intell. Expert* **1991**, *6*, 47–51.